Solar Energy Materials & Solar Cells 72 (2002) 403–416

Solar Energy Materials & Solar Cells

www.elsevier.com/locate/solmat

Oxygen and lattice distortions in multicrystalline silicon

H.J. Möller[a,*], C. Funke[a], A. Lawerenz[a], S. Riedel[a], M. Werner[b]

[a] Institute for Experimental Physics, Technical University Bergakademie Freiberg, Silbermannstr. 1, 09599 Freiberg, Germany

[b] Max-Planck Institute for Microstructure Physics, Weinberg 2, 06120 Halle, Germany

Abstract

Oxygen is one of the main impurities in multicrystalline silicon for photovoltaic applications. Precipitation of oxygen occurs during crystal growth and solar cell processing. It is shown that dislocations enhance the oxygen precipitation. Depending on the thermal conditions and the initial oxygen content various types of SiO_2 + precipitates and oxygen related defects are observed and investigated by fourier transform infrared (FTIR) spectroscopy and transmission electron microscopy. The large area distribution of oxygen decorated dislocations is studied by scanning infrared microscopy (SIRM). Both inhomogeneous distributions of dislocations and oxygen precipitates occur and can lead to internal stresses. The internal stresses of multicrystalline-silicon wafers are investigated by an optical method using polarized infrared light. The results are compared with the dislocation microstructure and the oxygen distribution in wafers produced by different growth techniques.
© 2002 Elsevier Science B.V. All rights reserved.

Keywords: Solar-silicon; Interstitial oxygen; Oxygen-precipitation; Dislocations; Internal stresses

1. Introduction

Multicrystalline silicon is a low-cost material for photovoltaic applications. The solar conversion efficiencies of commercial cells are typically in the range of 12–15% and up to about 17% have been obtained by sophisticated solar cell designs [1]. An improvement of the efficiency would greatly increase the commercial viability, if the production costs can be kept low at the same time. For multicrystalline solar cells the

*Corresponding author. Fax: 49-3731-394314.

E-mail address: moeller@physik.tu-freiberg.de (H.J. Möller).

0927-0248/02/$ - see front matter © 2002 Elsevier Science B.V. All rights reserved.
PII: S0927-0248(01)00188-X

material costs of the silicon are an important factor. Therefore, the material has to be used as efficiently as possible during all processing steps and losses as sawing, etching and fracture have to be kept low. The requirement to increase the material yield has become an increasingly important factor in recent years and many of the processing steps have been analyzed in view of the yield. One aspect is the loss of material due to breakage that occurs if stresses during handling the wafers or by thermal treatments exceed the fracture strength. Investigations of the fracture properties of multicrystalline silicon have shown that they also depend on the material quality. Silicon wafers produced by different techniques such as Cz- or Tri-crystal growth, ingot casting or by ribbon growth exhibit different fracture properties. It is, therefore, important to investigate the factors that determine the fracture properties.

Our investigations in recent years have shown that the surface quality, such as roughness and subsurface damage, in combination with internal stresses has to be considered. The origin of the internal stresses in multicrystalline wafers is not yet clear. In general, one can assume that it is produced by defects that lead to lattice distortions. In particular, we focused on the role of dislocations and oxygen that are known to lead to a substantial lattice distortion.

Dislocations are formed during crystal growth to reduce the thermal stresses by plastic deformation. Experimental investigations have shown that different growth techniques yield different dislocation structures. While crystals grown by directional solidification show rather homogeneous distributions of dislocations, ribbon growth techniques such as the EFG-method or the Tri-crystal growth technique produce rather localized dislocation arrangements. The internal stress levels and distributions are different and can partly be related to the dislocation substructure in the latter cases.

The concentrations of oxygen in ingot and Tri-silicon are comparable to Cz-silicon while the carbon concentrations are usually higher. The high concentration of interstitial oxygen leads to precipitation during crystal growth and the subsequent thermal processing steps. Both interstitial oxygen and its precipitates are accompanied by lattice dilatations and internal stresses. Oxygen can form a variety of defects. Clusters of a few oxygen atoms and larger SiO_2 precipitates of various sizes and crystal structures are observed [2,3]. Well-known defects are the Thermal Donors that are clusters of a few oxygen atoms and the New Donors that have been connected with SiO_2 precipitates [4]. These defects have been mainly studied because of their electrical properties but may also be important for the mechanical properties of multicrystalline silicon.

The evolution of the oxygen defects depends very much on the thermal history of the material and every thermal step between crystal growth and solar cell process has to be considered. In previous investigations, we have studied the bulk oxygen precipitation in multicrystalline silicon systematically [5,6]. The results have also shown that grain boundaries and particularly dislocations can enhance the oxygen precipitation significantly. Interstitial oxygen is also known to reduce the mobility of dislocations, which will affect the dislocation nucleation and multiplication during crystal growth. In view of the mechanical properties it is therefore important to study the interaction of dislocations with oxygen and the impact of the dislocation

structure on the internal stresses and crack nucleation. This paper summarizes some results on the oxygen precipitation at dislocations and their relationship to internal stresses.

2. Experimental procedure

2.1. Specimen preparation and defect characterization

Boron-doped multicrystalline silicon grown by directional solidification and EFG-ribbons were used for the investigations. The boron concentration was about $10^{16}\,cm^{-3}$. The oxygen and carbon concentrations of the wafers varied between $0.8–10 \times 10^{17}$ and $0.05–5 \times 10^{17}\,cm^{-3}$, respectively. Some of the as-grown wafers were annealed under argon gas at 1280°C for 2 h to dissolve the oxygen precipitates and determine the total initial oxygen concentration.

The dislocation densities were determined by selective etching on mechanically polished surfaces. The optical microscope images were recorded by a digital camera and the etch pits counted by an image processing system. In this way large areas with several thousand images could be analyzed automatically in a reasonable amount of time. This is necessary to obtain a statistically reliable correlation with other topographical results. The dislocation densities vary between $10^4–10^6\,cm^{-2}$ and locally up to $10^8\,cm^{-2}$.

2.2. SIRM and TEM investigations

The size, morphology and structure of the oxygen precipitates were investigated by conventional and high-resolution transmission electron microscopy (TEM, HREM). In some cases, the oxygen distribution was analyzed by energy filtered. TEM (EFTEM) allows the investigation of very small areas in the micron range only. The distribution of precipitates and dislocations varies however on a larger scale. In order to study the large-area distribution of oxygen precipitates, the scanning infrared microscopy technique (SIRM) has been applied. An infrared laser beam is focused in the specimen and scanned over an area of $100 \times 100\,\mu m$. The transmitted signal is recorded and converted into an image. The diameter of the focused beam is about 5 μm, the focal depth 30–50 μm. Topographical images over large areas of several millimeters are obtained by moving the scanning area. In addition, if the focus is moved in the beam direction, the entire volume of the specimens can be investigated. The specimen thickness can vary between 0.3–5 mm. It is estimated that precipitates larger than about 20 nm can be detected.

2.3. FTIR investigations

The concentrations of dissolved oxygen and carbon were determined by FTIR. Interstitial oxygen and substitutional carbon in silicon are associated with optical absorption lines at 1107 and $605\,cm^{-1}$, respectively. The concentrations of the

elements have been determined from the peak height using the calibration factors: 3.14×10^{17} and $1.0 \times 10^{17}\,cm^{-3}$, respectively. In addition, a broader line at $1224\,cm^{-1}$ can occur in the spectrum. This line has been associated with oxygen precipitates [7,8] and explained by the excitation of the LO-mode of SiO_2. The LO-mode is normally infrared inactive for bulk SiO_2 but can become active for particles that are small enough to become electrically polarized. Calculations of the polarization show that the $1224\,cm^{-1}$ band arises if the particles are smaller than $\lambda/2\pi n_m$, where λ is the wavelength of the incident radiation and n_m the refractive index of the embedding matrix, and have a plate-like shape [8]. The size, density and morphology of the oxygen and of carbon precipitates have been studied and confirmed by TEM.

2.4. Topographic stress measurements

The local internal stresses were measured by an optical double diffraction technique using a commercially available system. A circular polarized infrared laser beam is scanned over the wafer. The resulting polarization of the transmitted beam is measured and related to the internal stresses inside the wafers. Normally conventional wafers with a thickness of about 300–400 μm have been measured, but thicker wafers up to several millimeters could be investigated as well. The theoretical analyses show that the following information about the components of the stress tensor can be obtained: the difference of the main stress components in the wafer plane $\sigma_1 - \sigma_2$, and the direction of the long axis of the tensor ellipsoid. The stress component along the beam direction cannot be measured but is probably small in a thin wafer. The best resolution of the system is $200 \times 200\,\mu m^2$. The stresses are thus averaged over a relatively large volume. Therefore, the method allows one to study the long-range stress fields of the defects only. Measurements of the internal stresses of multicrystalline ingot or Tri-crystal silicon were done on polished wafers to avoid the stresses arising from the surface damage of as-cut wafers. For the EFG-ribbons polishing was unnecessary because of the damage-free surfaces.

3. Results and discussion

3.1. As-grown multicrystalline ingot silicon

Most of the following results have been obtained for multicrystalline ingot silicon and therefore, shall be discussed first. During solidification the planar melt interface moves from the bottom to the top of the ingot. Typically the oxygen concentration decreases from bottom to the top of the ingots and is particularly high at the bottom (Fig. 1). On the contrary, the concentration of carbon and many other impurities increases from bottom to the top. Depending on the oxygen concentrations and the cooling rates, particularly in the temperature range between 800°C and 1200°C when the diffusivity is still sufficiently high, oxygen may partly precipitate during cooling [6]. Oxygen precipitation is most likely in the bottom part where the concentration is

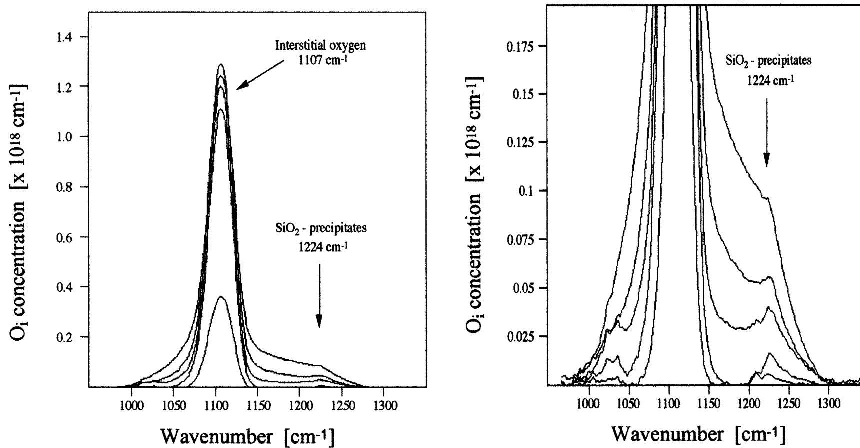

Fig. 1. FTIR spectrum of oxygen at various heights in a multicrystalline-silicon ingot. The spectra show the occurrence of precipitated SiO_2 in different concentration. (a) The lower peak heights at $1224\,cm^{-1}$ correspond to less oxygen; (b) In the upper part of the ingots.

higher. An example is given in Fig. 1 that shows the typical $1224\,cm^{-1}$ band for SiO_2 precipitates. The corresponding concentration of interstitial oxygen in this case shows that more precipitates are formed in as-grown samples when the interstitial oxygen concentration is higher. However, dislocations and carbon atoms can enhance oxygen precipitation and have to be considered as well (see Section 3.2). At present, it is not possible to calibrate the peak height with a quantity that characterizes the precipitate such as the density, size or shape of SiO_2 precipitates. Therefore, the amount of precipitated oxygen has to be determined differently (see Section 3.4).

3.2. TEM investigations

TEM investigations of the same specimens were performed to study the structure of the precipitates in the as-grown and annealed specimens. Basically two types of bulk precipitates are observed: spherical and plate-like defects [6]. Lattice images confirm the amorphous structure of the spherical defects that are typical for SiO_2 precipitates formed at higher temperatures in Cz-silicon. The sizes vary between 10–100 nm depending on the annealing conditions. The plate-like defects on (1 1 1) planes have a lateral extension up to 100 nm and a thickness of one or two atomic layers. Both spherical and plate-like defects can occur already in the as-grown multicrystalline material with densities up to $10^{11}\,cm^{-3}$ depending on the initial oxygen concentration and the thermal conditions during crystal growth. The density increases after annealing in the temperature range between 700°C and 1150°C and can reach maximum values of 10^{12}–$10^{13}\,cm^{-3}$ at around 950°C. Above 1050°C more spherical precipitates are observed and the $1224\,cm^{-1}$ absorbance line in the FTIR spectra disappears. This could be explained if the plate-like defects contain in fact

amorphous SiO_2 that causes the absorption. The transition from plate-like to spherical SiO_2 precipitates at higher temperatures is also observed in Cz-silicon.

Dislocations are preferred nucleation sites for oxygen. In fact most of the dislocations are decorated with oxygen precipitates (Fig. 2). Clusters of smaller amorphous precipitates are arranged along the dislocation line. The typical cluster sizes are between 50–100 nm, but the precipitates inside are much smaller, possibly only a few nanometers. The density and extension of the precipitates varies depending on the amount of precipitated oxygen. Energy filtered TEM (EFTEM) images confirm the enrichment of oxygen. In the bottom region with higher oxygen concentrations precipitation occurs both in the bulk and at dislocations. In the upper part of the ingots, with oxygen concentrations below $2 \times 10^{17}\,cm^{-3}$, the bulk precipitation ceases but precipitation at dislocations still occurs. This is in agreement with previous investigations in Cz- and multicrystalline silicon. The size of the clusters and the amount of precipitated oxygen are, however, smaller compared to the bottom region. The TEM investigations thus seem to indicate that most of the dislocations are decorated with oxygen precipitates in the ingot material. However, due to the small areas that can be studied and the large fluctuations in dislocation densities and probably impurity distribution, it became important to analyze the decoration with oxygen also on a larger scale. This became possible with the SIRM method as will be shown in the next section.

3.3. Scanning infrared microscopy investigations

Fig. 3 shows a typical SIRM image of a specimen in the lower part of the ingot showing several decorated dislocations extending over several hundred micrometers. The image shows an inhomogeneous decoration over the entire length and one can assume that the oxygen precipitates are responsible for the contrast. Some of the dislocations appear to have a weaker contrast. They are only out of focus because of their position in the wafer. This can be confirmed by moving the focus through the wafer, as is shown in a series of images in Fig. 4. The contrast becomes sharper when

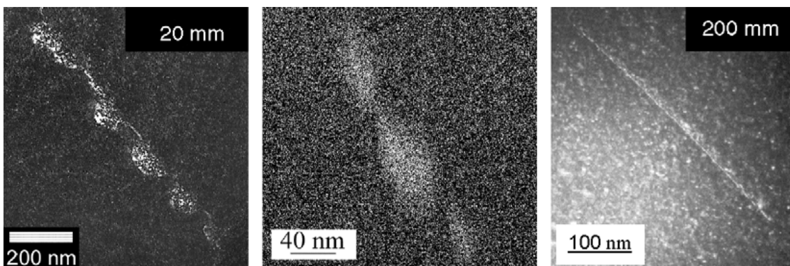

Fig. 2. (a) Weak-beam TEM image of amorphous SiO_2 precipitates at dislocations in the lower part of a multicrystalline-silicon ingot (at about 20 mm from the bottom). (b) The corresponding EFTEM image shows that the precipitates at the dislocation contain oxygen. (c) The amount of oxygen precipitation at dislocations in the upper part of the ingots is lower (at 200 mm).

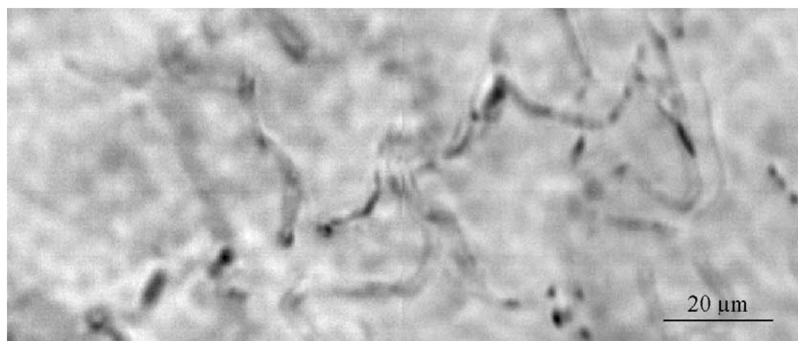

Fig. 3. Scanning infrared image of a dislocation in the oxygen-rich lower part of a multicrystalline-silicon ingot wafer. The contrast arises from the decoration with oxygen precipitates. The faint contrasts occur for out-of-focus dislocations.

Fig. 4. Scanning infrared images of the same dislocation with the beam focused at different depths in the wafer along the beam direction. The distance between the different positions of the focus is about 50 μm. The sharpest contrast (right image) occurs when the dislocation lies in the focal plane.

the dislocations lies in the focal plane. The technique thus allows one to study the degree of oxygen precipitation at dislocations over large volumes of the crystal.

The results show that indeed most of the dislocations are decorated. Bulk precipitation is rarely observed only in the lower part of the ingot (with higher oxygen concentration). The following quantitative results show however that bulk precipitation also occurs in this region (see Section 3.4). This indicates that these precipitates must be smaller, below the detection limit of the method (<20 nm). The distribution of the precipitates is inhomogeneous and correlated with the inhomogeneous distribution of the dislocations. With increasing ingot height and lower oxygen concentration, precipitation occurs only at dislocations in agreement with the TEM and quantitative FTIR investigations. Since less oxygen precipitates at the dislocations the SIRM contrast is reduced. Then, the dislocations are barely visible in the upper part of the ingots (Fig. 5). The intensity of the contrast only gives a qualitative impression of the amount of precipitated oxygen. In view of the importance of the dislocations for the electrical and mechanical properties of the material the amount of precipitated oxygen had to be determined quantitatively. This will be discussed in the next section.

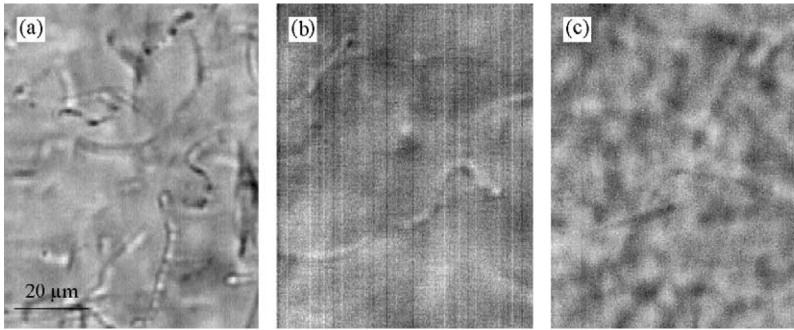

Fig. 5. SIRM images of oxygen-decorated dislocations from different positions in an multicrystalline silicon ingot: (a) 70 mm, (b) 140 mm, (c) 210 mm from the bottom of the ingot. The corresponding interstitial oxygen concentrations vary between 8–0.8 × 10^{17} cm^{-3}. (The blurred background in the images (b) and (c) is due to the increased background noise of the images.)

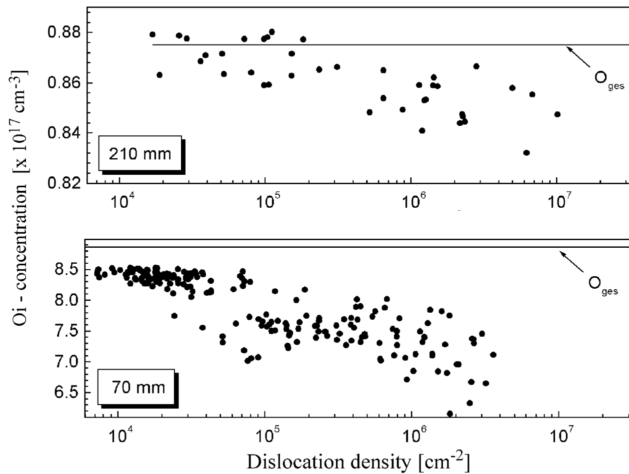

Fig. 6. FTIR measurements of the concentration of interstitially dissolved oxygen as a function of the dislocation density. Measurements are taken at two different positions of the multicrystalline ingot: at 70 and 210 mm from the bottom.

3.4. FTIR investigations

FTIR measurements allow one to determine the distribution of interstitial oxygen in the specimens quantitatively. Some of the results are shown in Fig. 6 for two different positions in the ingot. It can be seen that less dissolved oxygen occurs in regions of higher dislocation densities. Assuming that initially the oxygen concentration was homogeneous throughout the entire ingot, one can conclude that in regions of higher dislocation densities more oxygen is precipitated. This is in agreement with the previous qualitative results. The amount of precipitated oxygen

however cannot be determined directly. Some of the factors that hamper the analyses have been discussed before.

In addition, some of the oxygen probably is also precipitated in small clusters that are not visible even by the HREM technique. Since the interstitially dissolved oxygen can be determined quite accurately, the following procedure has been applied to determine the total amount of precipitated oxygen. The specimens with precipitates were annealed at such a high temperature that all precipitates and cluster were dissolved again. For the range of oxygen concentrations a temperature of 1280°C and an annealing time of 2 h was sufficient. After annealing the specimens where cooled down quickly to avoid the renewed precipitation. Measuring the dissolved interstitial oxygen concentration before and after the annealing treatment allows one to determine the amount of precipitated oxygen from the difference of both measurements. The measured oxygen concentration in the annealed specimens is also shown in Fig. 6. It indeed shows that it is uniform in all regions but varies with the height of the ingot.

For low dislocation densities in the as-grown wafers, a saturation value is obtained which differs from the total value in the annealed specimens at least in the lower part of the ingot. This is due to the bulk precipitation, which does not occur in the upper part because of the lower total oxygen concentration (below $2 \times 10^{17}\,cm^{-3}$). The difference between the total concentration and the concentration in the as-grown wafers yields the total amount of precipitated oxygen. In order to determine the amount of oxygen that precipitated at the dislocations one only has to take the difference between the saturation value for low dislocation densities and each value. This is based on the assumption, however, that the amount of bulk precipitation is the same in regions of low and high dislocation densities. In the upper part (at 210 mm in Fig. 6) where no bulk precipitation occurs both values are the same. The result of the procedure is shown in Fig. 7 where the amount of precipitated oxygen per unit length of the dislocation is plotted versus the dislocation density.

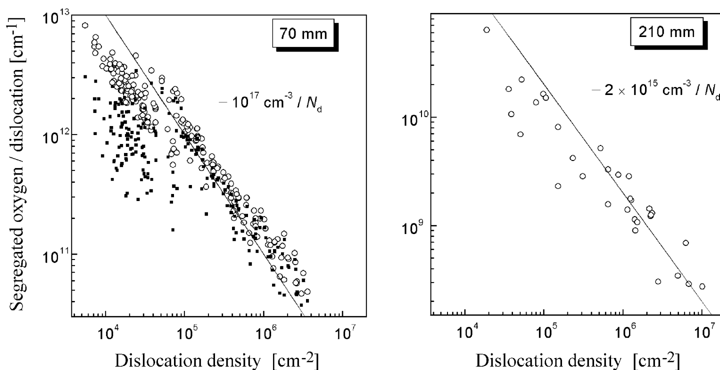

Fig. 7. FTIR measurements of the concentration of interstitially dissolved oxygen as a function of the dislocation density. Measurements are taken at two different positions of the multicrystalline ingot: at 70 and 210 mm from the bottom. Open circles correspond to the total amount of precipitated oxygen, filled circles to the amount of oxygen precipitated at dislocations.

It shows that less oxygen precipitates per dislocation length with increasing dislocation density. This can be explained under the assumption that the dislocations compete with each other for the interstitial oxygen that is available in the bulk, even for the low-oxygen concentrations of $0.8 \times 10^{17}\,cm^{-3}$ in the upper part. Without competition the same amount of oxygen per unit length should be observed, independent of the dislocation density. In summary, one can say that the dislocations in regions of higher dislocation densities are thus much less decorated with oxygen. The total amount of precipitated oxygen is however higher. These results have to be considered if the corresponding lattice distortions and internal stresses are analyzed in the following section.

3.5. Internal stresses

Dislocations, interstitial oxygen atoms, and oxygen precipitates are accompanied by local lattice distortions due to the elastic strain field of the dislocations and the lattice mismatch (volume expansion) of the oxygen atom and its precipitates. Particularly, the lattice distortions of oxygen precipitates have been studied extensively in the past in Cz-silicon (For example, see [9]). One of the results is that the lattice dilatations around oxygen precipitates can be reduced by a variety of processes such as the emission of interstitial silicon atoms or the punching out of dislocation loops. In addition, the precipitates may assume a shape that reduces their strain. Much less is known however about the oxygen behavior in multicrystalline silicon, but our previous [6] and the present results show that there are differences in this material such as the precipitation at dislocations. Basically two types of precipitates have been observed in multicrystalline silicon: plate-like precipitates at lower temperatures (mainly at $T < 800^{\circ}C$) and spherical, amorphous precipitates at higher temperatures ($> 900^{\circ}C$). Since most of the spherical precipitates occur at dislocations, the punching out of dislocation loops or the emission of self-interstitials cannot be observed or may not even occur. One can assume however, that the strain field of these precipitates is partly reduced by precipitation at the dislocations. The bulk precipitates in the material are either smaller or have a plate-like shape. In both cases their stress fields should be higher [10].

Areas of higher densities of dislocations or of oxygen precipitates can thus lead to long ranging strain fields and internal stresses. Although the local stresses may be quite high, for instance near the core of a dislocation, the long ranging stress fields can be very different due to the interaction of the strain fields. For instance in dislocation pile-ups the stresses at the front can become very high, whereas the stress fields of homogeneously distributed dislocations may cancel each other and result in overall low stresses. In view of the mechanical fracture properties it is unclear yet whether the local internal stresses on a scale below a few micrometers or the distributions of stresses on a larger scale have to be considered. In the following, the long-range stress fields have been measured only because of the limited lateral resolution of the applied measuring technique of about $200\,\mu m$. Local stress concentrations in a smaller region are thus not detectable by this method.

Fig. 8 shows the results of the internal stress measurements of a multicrystalline etched wafer. The measurements were taken with the highest resolution. The results show a rather homogeneous distribution of stresses without much structure in the stress range of 1–3 MPa. The corresponding optical image of the etched surface showing grain boundaries and the etch pits from the dislocations is given on the left side. Since the visual comparison does not show a clear correlation between dislocated regions and the stress pattern, the images were analyzed quantitatively. Corresponding regions of about $2 \times 2\,\text{mm}^2$ were taken and the local stress and dislocation density values averaged. The results are depicted in Fig. 9 and show that there is no unique correlation between stresses and dislocation density. However, the tendency can be observed that for low dislocation densities most of the highest stress values are found.

This result is typical for wafers grown by the ingot technique that produces in general lower internal stresses. In comparison, wafers from EFG-ribbons or Tri-crystals exhibit a less uniform stress distribution and locally higher stresses. An example is shown in Fig. 10. High local stresses correspond to high dislocation densities here. The stresses in these areas are about five times higher and dislocation

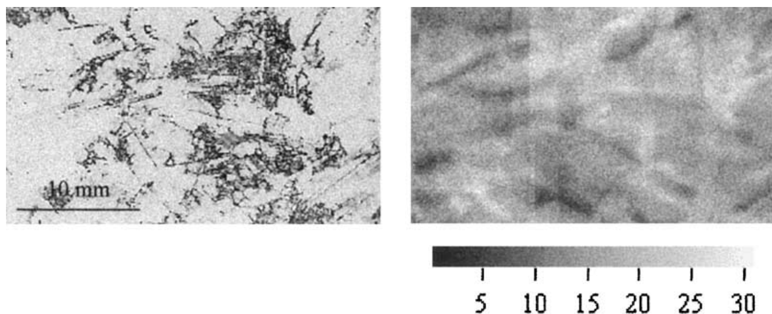

Fig. 8. Optical image of the etched surface of a multicrystalline wafer showing etch pits of dislocations and grain boundaries (left). Topographical image of the internal stress distribution of the same area (right) (the stress scale is given in units of 0.1 MPa). The optical birefringe technique has a resolution of 200 μm.

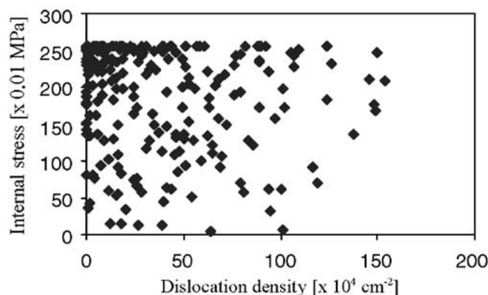

Fig. 9. Correlation of the local internal stress and the dislocations density. The values are averaged over a square area of $2 \times 2\,\text{mm}^2$ (stresses above 2.5 MPa are not resolved).

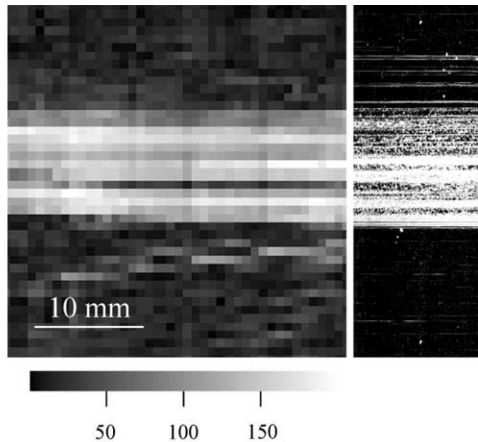

Fig. 10. Topogram of the internal stresses (left) and the corresponding optical image of the etched surface of the same area (right) showing dislocation etch pits and twin Lamellas for a EFG wafer. (stress scale in 0.1 MPa units).

densities of up to $10^8\,cm^{-2}$ are observed. Similar results are obtained for Tri-crystal silicon, which can also show a rather localized dislocation structure with higher internal stresses. The contamination of the dislocations with oxygen precipitates has not been investigated, but one can assume that in EFG silicon much less decoration occurs because of the lower oxygen concentration ($<10^{17}\,cm^{-3}$).

The different internal stress patterns that are observed in ingot and EFG silicon may be explained in the following way. The analyses of the dislocation structure shows that in the ingot technique dislocation multiplication occurs by slip on several glide planes in each grain (multiple slip), similar to the plastic deformation of a polycrystal. This produces a rather uniform dislocation network with different types of dislocations. The dislocations are, therefore, most likely distributed in such a way that their stress fields more or less cancel each other on a scale, which is larger than their mean distance (for $N_d = 10^6\,cm^{-2}$ about 10 μm). The reduction of the local thermal stresses by plastic deformation and the organization of the dislocations into a strain-poor configuration will be easier at high temperatures ($>1000°C$), when the dislocations are more mobile. The dense dislocation networks (with $N_d > 10^5\,cm^{-2}$) produce many nucleation sites for the oxygen and precipitation mainly occurs at the dislocations. These precipitates probably do not contribute significantly to the strain so that these areas mainly exhibit low internal stresses.

The situation for the areas of lower dislocation densities (with $N_d < 10^5\,cm^{-2}$) is different. Lower dislocation densities should produce lower internal stresses. On the other hand, more oxygen will precipitate in the bulk then at least for higher oxygen concentrations (in the lower part of the ingot). The SIRM results have shown that these precipitates are smaller which should produce higher stresses according to previous investigations on Cz-silicon [10]. In addition, if the low-density areas have formed at lower temperatures when dislocation mobility is low, more plate-like precipitates will have formed which may also produce higher stresses. The observed

higher stresses in some of the low-density areas in ingot silicon are therefore due to the precipitation of oxygen in the bulk. The stress pattern in ingot silicon is thus determined by several factors, which may explain the wide scattering of data points in Fig. 9.

In the EFG-ribbons, slip mainly occurs on one set of glide planes (single slip) which produces a high density of dislocations of the same type on parallel planes. In such an arrangement of dislocations the strain fields cannot cancel each other and thus produces higher stresses. In the dislocation-free regions no significant oxygen precipitation occurs because of the lower oxygen concentration, therefore these areas remain mainly strain free. The EFG material is thus characterized by high local strains due to the special dislocation arrangement and a high density of twin boundaries. A similar situation may occur for Tri-crystal silicon where dislocations are also generated locally on a few slip systems.

4. Summary and conclusions

Experimental results have been obtained about the distribution of dislocations and oxygen precipitates in multicrystalline ingot and EFG silicon. The observations can qualitatively explain the measured internal stress distribution in as-grown wafers. Both the arrangements of dislocations and of the dilatation stresses the oxygen bulk precipitates have to be taken into account. In view of the fracture strength the following conclusions can be drawn.

Preliminary results on the fracture strength of multicrystalline wafers, which will be published later, indicate that two factors have to be considered: microcracks or other stress enhancing inhomogeneities (e.g. roughness) at the surfaces and internal stresses. The first factor is mainly important for wafers that are cut by sawing such as ingot and Tri-silicon. These materials are mainly fragile because of a high density of microcracks. After removal of the saw damage by etching, other factors such as surface roughness and the internal stresses become more important. This may explain that EFG-ribbons which have almost no saw damage apart from the edges but shows very localized higher internal stresses, is rather fragile. On the contrary, ingot silicon with a rather homogeneous distribution of dislocations and lower stresses has a higher fracture strength.

Acknowledgements

Part of the work has been supported by the German BMBF under the contract numbers 0329858K and 0329745A. One author (M.W.) would like to thank Dr. E. Pippel (MPI for microstructure Physics, Halle) for his help in applying the EFTEM technique.

References

[1] J.M. Gee, R.R. King, K.W. Mitchell, 25th IEEE Photovoltaic Specialists Conference, Washington, DC, 1996, p. 409.
[2] W. Bergholz, Semiconduct. Semimet. 42 (1994) 513.
[3] A. Borghesi, B. Pivac, A. Sassella, A. Stella, J. Appl. Phys. 77 (9) (1995) 4169.
[4] J. Michel, L.C. Kimmerling, Semiconduct. Semimet. 42 (1994) 251.
[5] H.J. Möller, M. Ghosh, S. Riedel, M. Rinio, D. Yang, 13th European Photovoltaic Solar Energy Conference, 1995, p. 1390.
[6] H.J. Möller, L. Long, D. Yang, M. Werner, Phys. Stat. Sol. A 171 (1999) 175.
[7] F. Shimura, H. Tsuya, T. Kawamura, Appl. Phys. Lett. 37 (1980) 483.
[8] S.M. Hu, J. Appl. Phys. 51 (1980) 5945.
[9] Oxygen, carbon, hydrogen and nitrogen in crystalline silicon. Mat. Res. Soc. Symp. Proc. 59 (1986) (Eds. J.C. Mikkelsen, S.J. Pearton, J.W. Corbett, S.J. Pennycock), Semiconductors and semimetals, vol. 42. New York: Academic Press, 1994; Defects in silicon II. The Electrochemical Society, 1991 and references therein
[10] V.V. Balatov, M.D. Efremov, I. Babanskaya, K. Schmalz, Mater. Sci. Eng. B 21 (1993) 49.